Measured and Simulated Acoustic Signature of a Full-Scale Aircraft with Airframe Noise Reduction Technology Installed

Mehdi R. Khorrami[1]
NASA Langley Research Center, Hampton, VA, 23681, USA

Patricio A. Ravetta [2]
AVEC Inc., Blacksburg, Virginia 24060, USA

David P. Lockard[3]
NASA Langley Research Center, Hampton, VA, 23681, USA

Benjamin Duda[4]
Dassault Systèmes, D-80637 Munich, Germany

Ryan Ferris[5]
Dassault Systèmes, Long Beach, California, 90802, USA

Microphone phased-array and pole-mounted microphone data gathered during the NASA Acoustics Research Measurements flight tests were used to benchmark results from companion full-scale aeroacoustics simulations. Conducted with the lattice Boltzmann solver PowerFLOW®, the simulations predicted the acoustic behavior of various tested aircraft configurations. Emphasis was placed on those flown during the third flight test - a Fowler flap-equipped Gulfstream G-III with and without noise abatement technology on the main landing gear. Direct comparisons between experimental and synthetic microphone phased-array data were achieved by applying the same processing and deconvolution technique to both sets of data. To extend the validation of the computations to the metric used for noise certification, the Effective Perceived Noise Level, a high-fidelity digital model of the nose landing gear, which was excluded from earlier computations, was developed and integrated into the G-III aircraft geometry. The acoustic study presented here demonstrates that the simulated beamform maps and corresponding integrated farfield spectra accurately predict the locations and strengths of the prominent airframe noise sources present on the G-III aircraft.

Nomenclature and Acronyms

ACTE = Adaptive Compliant Trailing Edge
AFRC = Armstrong Flight Research Center
AOA = Angle of attack
ARM = Aeroacoustics Research Measurements
EPNL = Effective Perceived Noise Level
FAA = Federal Aviation Administration
FWH = Ffowcs-Williams and Hawkings
ICAO = International Civil Aviation Organization
MLG = Main landing gear
NLG = Nose landing gear

[1] Aerospace Engineer, Computational AeroSciences Branch, Associate Fellow AIAA.
[2] Co-owner, Chief Research Engineer, Senior Member AIAA.
[3] Aerospace Engineer, Computational AeroSciences Branch, Senior Member AIAA.
[4] Senior Technical Specialist, Simulia A&D.
[5] Solution Consultant Specialist, Simulia A&D, Member AIAA.

NR = Noise reduction
PNL = Perceived Noise Level
PNLT = Tone-corrected Perceived Noise Level
SCRAT = SubsoniC Research Aircraft Testbed
SNR = Signal-to-noise ratio
SPL = Sound Pressure Level

I. Introduction

Considerable progress in aircraft noise abatement has been made since the advent of jet-powered civil aviation. Most of the early achievements were in the reduction of engine noise, as this was, by far, the dominant component. The development of relatively quiet, high-bypass ratio powerplants highlighted the importance of nonpropulsive sources of noise. During landing, when the undercarriage and wing high-lift devices are deployed, airframe noise is the most important contributor to the farfield acoustic signature of most modern aircraft [1]. Due to the geometric intricacies of airframe components, the noise they produce is broadband in nature and spans a wide frequency range. These characteristics have made the system-level simulation of airframe noise a very difficult and elusive problem. Relatively new techniques for the simulation of complex fluid systems have facilitated the prediction of airframe noise for full-scale aircraft and the assessment of noise mitigation technologies [2-7]. To foster their widespread use for realistic applications within the aviation industry, computational methodologies must be robust with predictive capabilities rigorously validated with high-quality measurements obtained in relevant flight environments.

The purpose of the Aeroacoustics Research Measurements (ARM) flight tests, which were executed under the Flight Demonstrations and Capabilities project of the NASA Integrated Aviation Systems Program, was twofold: to evaluate the aeroacoustic performance of several airframe noise reduction (NR) technologies as installed on a Gulfstream G-III aircraft, and to generate a comprehensive aeroacoustics database for the advancement of simulation-based airframe noise prediction methods. All ARM flights were conducted with two G-III aircraft based at the NASA Armstrong Flight Research Center (AFRC). A stock G-III aircraft, also known by its tail number as "808," served as the initial baseline configuration. However, the primary G-III used during the ARM tests was the SubsoniC Research Aircraft Testbed (SCRAT), also known by its tail number as "804." The heavily instrumented 804 allows in-flight recording of aircraft parameters such as global position, angle of attack (AOA), and true airspeed. The Adaptive Compliant Trailing Edge (ACTE) flap was evaluated as a mechanism to reduce flap noise during the first test (ARM-I, 2016) [8, 9]. The second flight test (ARM-II, 2017) [8, 9] focused on assessing the effectiveness of various main landing gear (MLG) and gear cavity treatments in conjunction with the ACTE technology. For the third flight test (ARM-III, 2018), the ACTE flaps were removed and the original Fowler flaps were reinstalled on the G-III to obtain baseline flap and landing gear data, and to assess the NR capability of the landing gear technologies for conventional flaps [10]. Extensive acoustic measurements were acquired with a NASA-developed microphone phased-array system [11] and certification-type, pole-mounted microphones [12] during the ARM flight tests.

Comparative analyses between simulated and measured aeroacoustic data generated during the ARM-I and ARM-II flight tests were presented in Ref. [13]. These simulations excluded the nose landing gear, and the comparison focused on phased array data used to isolate the noise from the flaps and main gear. Good agreement of the farfield noise signature of the G-III aircraft with ACTE flaps, with and without landing gear deployed, was observed between the two data sets. Those results demonstrated that: 1) application of the ACTE technology drastically reduces aircraft flap noise, and 2) the MLG treatments are very effective at reducing noise from the main gear and the wheel cavity. In this paper, we focus on the acoustic performance, both measured and simulated, of the MLG treatments in combination with conventional (Fowler) flaps. Of paramount importance to the industry is the metric used for aircraft certification, the Effective Perceived Noise Level (EPNL). To further enhance and demonstrate the predictive capability of the present computational approach, we also extended validation of the synthetic (simulated) results to EPNL values determined from the certification microphone measurements obtained during the ARM tests. To facilitate comparisons, a high-fidelity representation of the nose landing gear (NLG) was developed and incorporated into the G-III aircraft digital model. Although the addition of the NLG enhances the physical fidelity of the computational model, we do not expect the synthetic levels to perfectly match measured EPNL values. The latter are affected by factors that are difficult to incorporate in a simulation, such as the presence of secondary noise sources (e.g., residual engine noise and tones generated by the wing fuel vapor vents) and background noise at the test site. Nevertheless, we believe that the EPNL comparison is an important additional step in the validation process of the present computational methodology.

II. Experimental and Computational Data Sets

The experimental data consist of extensive phased-array and pole-mounted microphone measurements obtained during the ARM flight tests [8, 10, 12] conducted by NASA. During these tests, a NASA Gulfstream G-III aircraft (Fig. 1a) was fitted with several airframe NR concepts and flown on an approach pattern at various flap deflection angles. The tested technologies comprised ACTE flaps, MLG fairings (Fig. 2a), and gear cavity treatments. A full account of the ARM flight tests, phased-array and pole-mounted microphone measurements, and NR technologies evaluated is presented in Refs. [8, 9, 10, 12].

The computational data were obtained from simulations of the full-scale aircraft with ACTE and Fowler flaps, with and without the MLG fairings (Fig. 2b), after the NLG was added to the G-III aircraft geometry (Fig. 1b). The lattice Boltzmann PowerFLOW® code was used to perform the time-accurate flow simulations at a Mach number of 0.23 and a Reynolds number (Re) of 10.5×10^6. The latter represents a value that is close to 60% of the flight Re based on a mean aerodynamic chord of 13.78 ft (4.2 m) and an aircraft speed of 150 knots. Formulation 1A [14], a solution to the acoustic analogy of Ffowcs-Williams and Hawkings (FWH) [15], was used to propagate the computed nearfield fluctuations to the farfield array microphone locations. The formulation was extended to account for uniform mean flow convection effects to simulate the noise generated and measured in an ideal infinite wind tunnel [16]. Aircraft solid surfaces and a FWH permeable surface (shown in Fig. 3 and described in Ref. [7]) were used to calculate the farfield acoustic footprint. The synthetic microphone array pressure records contain 1.5 s of simulated physical time. A description of the simulated configurations, computational approach, and computed data sets are provided in Refs. [5-7].

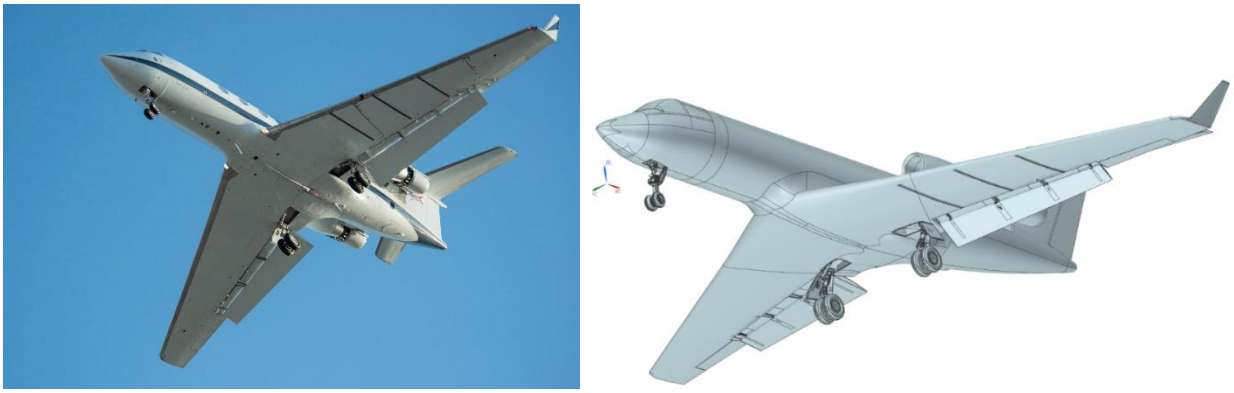

a) NASA G-III aircraft **b) CAD model**

Fig. 1 Gulfstream G-III aircraft with Fowler flaps. As flown aircraft (left image) and developed CAD geometry (right image).

a) **Tested physical model** **b) Simulated CAD geometry**

Fig. 2 Gulfstream G-III main landing gear with fairings installed. The faired gear is depicted in its stretched, in-flight state (from Ref. [13]).

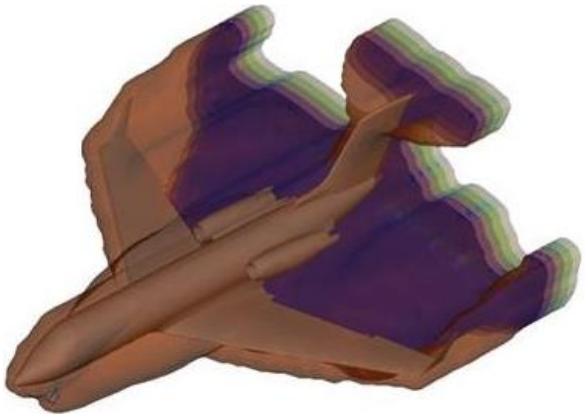

Fig. 3 Permeable surface (with multiple downstream endcaps) used during simulation as shown on the Fowler flap equipped G-III (from Ref. [7]).

A. Data Analysis

The processing approach applied to the current microphone array data sets is identical to that described in Ref. [13]. A summary is provided here for completeness.

The FWH propagation approach of Ref. [16] was used to generate synthetic pressure records at the same array microphone locations of the ARM flight tests. To facilitate direct comparisons and minimize potential differences, both measured and simulated pressure records were processed in a similar fashion. A time-domain, delay-and-sum beamformer with diagonal removal coupled with CLEAN deconvolution, available within AVEC's Phased Array software suite [17], was used to process the microphone array data collected during the ARM tests. The frequency-domain version of the same software [17] was used to process the synthetic array data. Although the measured and simulated data had different sampling frequencies, the spectral resolution for both sets was matched to allow a direct comparison of the narrowband acoustic maps and their corresponding integrated results. Beamform maps that provide the position and sound pressure level (SPL) of the acoustic sources were generated from the processed data on a square, 100 ft by 100 ft (30.5 m by 30.5 m) planar grid covering the entire aircraft. Following our previous study [8], a grid size of 201 × 201 points, representing a spatial resolution of 6 in. (15.25 cm), was chosen. As shown in Ref. [8], this resolution is adequate for proper source localization. The results presented here were scaled to an altitude of 394 ft. (120 m) under the assumption of spherical spreading for pressure ($p'^2 \sim 1/r^2$).

Three integration regions were used to isolate flap, MLG, and NLG contributions to the farfield noise and to assess the noise reduction performance of the tested landing gear technologies. These regions are highlighted in Fig. 4: 1) a delta-shaped region named "WingsNg" that excludes the contributions from the nose gear, wingtips and leading edges, and engines; 2) a small, rectangular region called "MLG" that contains the main landing gear; and 3) a second rectangular region called "NG" that contains only the nose landing gear component. The "WingsNg" region permitted us to determine the acoustic benefits of the landing gear technologies when the noise produced by the Fowler flaps was also included in the farfield spectrum. As described in Ref. [8], this integration region was tailored to exclude contributions from residual engine noise, tones from fuel vapor vents located near the wing tips and scattering of fan tones from the wing leading edges. The "MLG" region was used to assess the isolated effectiveness of the main gear fairings and cavity treatments by excluding a significant portion of the flap noise. Note that the current "MLG" region is larger in the downstream direction than a similarly named zone used previously [8]. Strong sources at the flap inboard tips produced inconsistent integrated spectral levels when using the initial, smaller "MLG" region, even for consecutive array passes of the same aircraft configuration. Thus, the "MLG" integration zone was enlarged to completely encompass the flap inboard tips. As demonstrated in Ref. [10], the integrated levels extracted from the larger "MLG" region yield very consistent and repeatable trends and values. The "NG'" region, isolating the front section of the fuselage, allowed us to computationally determine the noise generated by the NLG and how much this component contributes to EPNL values. Further discussions on the reasons for choosing the shape and extent of the "WingsNg" and "MLG" integration regions are included in Refs. [8] and [10], respectively.

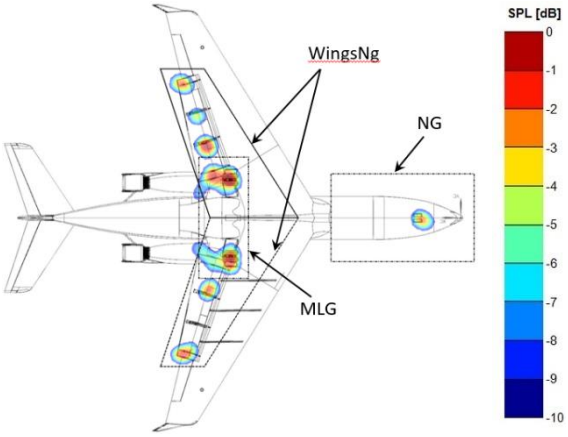

Fig. 4 Integration regions used to separate contributions from measured sources to the farfield noise spectrum. Sample acoustic map for Fowler flaps deflected 39° and landing gear deployed. Map generated using conventional beamforming.

Two similar but independent approaches were used to calculate EPNL values. The proprietary post-processing tool developed by Dassault Systèmes was used with the synthetic data set. The primary reference for the definition and calculation of EPNL is a publication of the International Civil Aviation Organization (ICAO) [18]. The input to the tool is a semicircular arc of synthetic pressure signals obtained by way of a Ffowcs-Williams and Hawkings (FWH) calculation. Once a trajectory is determined, it is discretized into flight segments of a given duration, in this case 500 ms. For every flight segment, the emission time and position of the aircraft is determined, and a ray between the observer and aircraft is traced. The ray's intersection with the semicircular microphone array is determined and a noise spectrum for the observer is formulated by interpolating the appropriate microphones' narrow-band spectra. The spectrum at the observation point is corrected for distance, atmospheric absorption, Doppler shifting and ground reflection for each flight segment. One-third octave sound pressure levels (SPL) are then computed and Perceived Noise Level (PNL) is calculated using the procedure described by ICAO. Finally, tonal weighting and band sharing adjustments are made and the EPNL is computed. An analogous approach implemented into AVEC's proprietary software was used to obtain EPNL values from the experimental data set. The approach is based on FAA Advisory Circular No. 36-4D [19], which is equivalent to the ICAO publication [18]. The steps used to process the pressure records measured with the certification microphones are described in detail in Ref. [12].

There are a few differences between the two methods used to calculate EPNL that stem from additional steps required to process experimental data. These steps are: 1) consideration of background noise at the test site; 2) adjustments to a reference path to account for variations in position, glide slope and speed in the flight path; and 3) inclusion of atmospheric attenuation corrections due to local meteorological conditions. To ensure that EPNL computations were equivalent, the simulated data set was also processed using AVEC's method. The results indicated that the levels were within 0.05 EPNdB.

III. Results and Discussion

Comparative analyses of measured and synthetic data produced for aircraft configurations flown during the ARM-I and ARM-II flight tests are provided in Ref. [13]. In the present study, we emphasize the validation of computed results with data from the ARM-III test [10]. The simulated configurations comprised the G-III aircraft with its Fowler flaps deflected at 20° and 39°, landing gear deployed, with and without MLG fairings installed. As mentioned earlier, the NLG geometry was added to the G-III CAD model to produce a more complete representation of the aircraft during approach and landing, and to facilitate direct comparisons between measured and predicted EPNL values. Table 1 contains the aircraft parameters/configurations that were chosen for the simulations presented here. For each configuration the parameters were carefully selected to match the aircraft states recorded during several array flyover passes. The NLG geometry was also added to the G-III aircraft equipped with ACTE flaps to simulate the configuration with MLG fairings installed. This updated configuration is being used to examine NLG effects on farfield noise signatures by revisiting some of the cases presented in Ref. [13]. To ascertain grid dependency, the simulations were conducted at mesh resolutions corresponding to coarse and medium density grids (see Ref. [7] for further details). Finer resolution simulations of a select few configurations could not be completed because of the

extended US federal government shutdown. These simulations are currently ongoing and the results will be presented in a future publication.

The results will be presented in three segments. Source localization (beamform) maps generated from the measured and simulated data are compared and discussed in the first segment. For each configuration, maps obtained from synthetic data are compared with experimental maps from multiple array passes for the same aircraft configuration conducted at the same conditions (e.g., AOA, glide slope). Comparison of the maps is restricted to a few frequencies within the low, medium, and near-high ranges of the spectrum. A qualitative assessment of MLG fairing performance for configurations with Fowler flaps is also provided in this section. Measured and predicted farfield spectra obtained from integration of the "WingsNg", "MLG", and "NG" regions are presented and discussed in the second segment. The acoustic performance of the MLG fairings in the presence of conventional Fowler flaps is determined and quantified. The last segment of this section is focused on EPNL comparisons between measured and simulated results. Emphasis is placed on how well the computations predict the relative reduction in EPNdB attained with the MLG fairings. Also highlighted are some of the challenges associated with prediction of absolute EPNL values. Unless stated otherwise, all predictions from medium-resolution simulations used pressures computed on aircraft solid surfaces.

Table 1. Aircraft conditions and parameters for simulated configurations.

G-III aircraft configuration				Aircraft parameters	
Flap type	Flap deflection angle	Landing gear deployed	Main gear fairings applied	Angle-of-attack (AOA)	Glide slope angle
Fowler	20°	Yes	No	5°	5°
Fowler	20°	Yes	Yes	5°	5°
Fowler	39°	Yes	No	2.85°	7°
Fowler	39°	Yes	Yes	2.85°	7°
ACTE	25°	Yes	No	4.65°	5.1°
ACTE	25°	Yes	Yes	4.65°	5.1°

A. Beamform Maps

All source localization (beamform) maps presented here were generated in $1/12^{th}$-octave bands. To achieve a direct comparison between simulated and measured maps, the amplitudes were scaled as follows: first, the SPLs for the experimental maps were normalized to 150 kts using V^6 scaling (see Ref. [10] for a discussion on velocity scaling selection). Then, at each frequency, the peak SPL value among the maps being compared was subtracted from the levels of all maps to create a common SPL range. This common SPL range – from peak level (0 dB) to 10 dB below the peak – was used for the beamform maps presented hereafter.

1. Approach Configuration

Sample beamform maps for the baseline case of Fowler flaps deflected 20° and landing gear deployed (approach configuration) are presented to illustrate how well the predicted results capture the trends observed from the flight test data. The landing gear is the dominant source at this lower flap deflection. Thus, a good estimate of the noise reduction performance of the applied MLG fairings can be obtained with this configuration. Simulated beamform maps and measured maps from two aircraft passes are presented in Fig. 5 for frequencies of 425 Hz, 1,120 Hz, 1,600 Hz, 2,240 Hz, and 3,150 Hz. At frequencies below 400 Hz, measured G-III airframe noise is dominated by tones from the fuel vapor vents near the wing tips and from the MLG cavity. As explained in Ref. [13], the fuel vapor vents were not included in our simulated geometry, neither were numerous smaller components found inside the actual cavity. At 425 Hz, the measured maps (Figs. 5a-5b) show that the MLG is the dominant source, followed by the NLG. Also apparent in the measured maps are secondary sources generated by the G-III aircraft engines, even though all passes were flown with engines set at ground-idle. As demonstrated in Ref. [8], these secondary sources contribute to the integrated spectral levels obtained from various regions, including those devised to minimize such contributions. The simulated map at 425 Hz (Fig. 5c) captured rather well the peak levels and relative strength of the landing gear sources. Good correspondence between measured and simulated sources extends to frequencies up to 1,200 Hz. At a frequency of 1,120 Hz (Figs. 5d-5f), the simulated map depicts the two MLG and the NLG sources to be dominant and of equal strength, in good agreement with the trends measured during pass 7 (Fig. 5e). Even though the flyover passes were consecutive, notice that the measured maps are not similar: the map for pass 6 (Fig. 5d) indicates that the levels for the starboard MLG were approximately 2 dB lower than those for the main gear on the port side. Discrepancies such as this are inherent to flight testing and in most instances are determined by the presence and magnitude of cross

winds. Thus, data from multiple aircraft passes are necessary for the proper assessment of airframe noise sources. At frequencies between 1,200 Hz and 2,000 Hz (Figs. 5g-5i), the simulated maps depict substantially underpredicted peak levels for the gear sources, even though the relative strengths of the MLG and NLG components were captured correctly. We attribute this behavior to insufficient spatial resolution in our medium-resolution simulation. What puzzles us, however, is that the agreement between predicted and measured maps improves drastically for frequencies between 2,000 Hz and 3,000 Hz. To illustrate this point, plotted in Figs. 5j-5l are maps for a frequency of 2,240 Hz. As can be seen from Fig. 5l, the location and strength of the major airframe sources were predicted accurately. Notice that, at this frequency, the flap brackets become secondary noise sources and were properly captured by the simulation. Also appearing in the measured maps are sources on the engine nacelles that are caused by air intakes for generator cooling. Adequate exclusion of contaminating noise sources from the integration regions is among the intrinsic difficulties that arise when comparing predicted and measured integrated farfield spectra: because of its close proximity to the wings, this engine source appears in both "WingsNg" and "MLG" integration regions and increases the spectral levels over a large range of frequencies. At frequencies above 3,000 Hz, the simulated peak levels appear to be underpredicted, even though the prominent sources are correctly identified (Figs. 5m-5o).

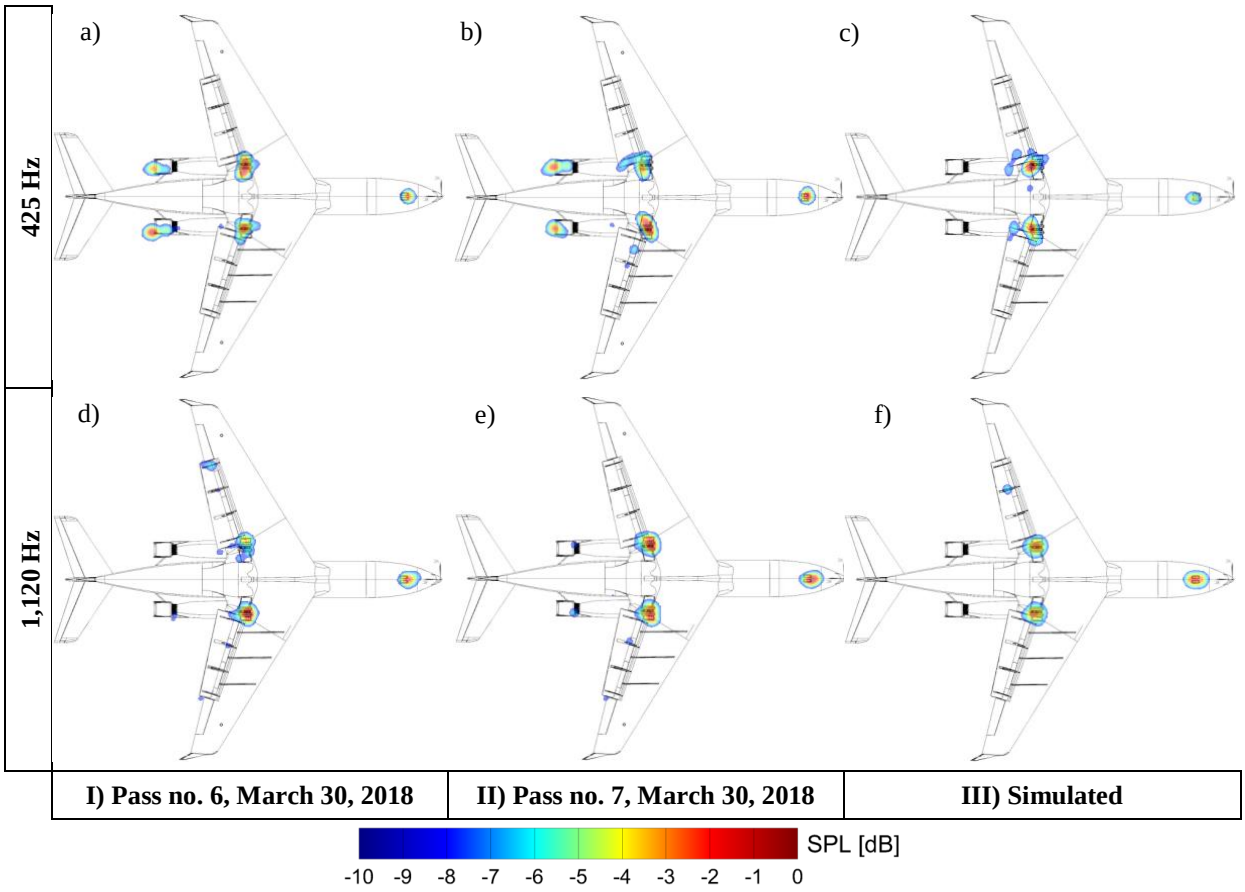

Fig. 5. Beamform maps for the 804 aircraft in landing configuration with flaps deflected at 20° and landing gear deployed, overhead position. From measurements (left two columns) and medium-resolution simulation (right column).

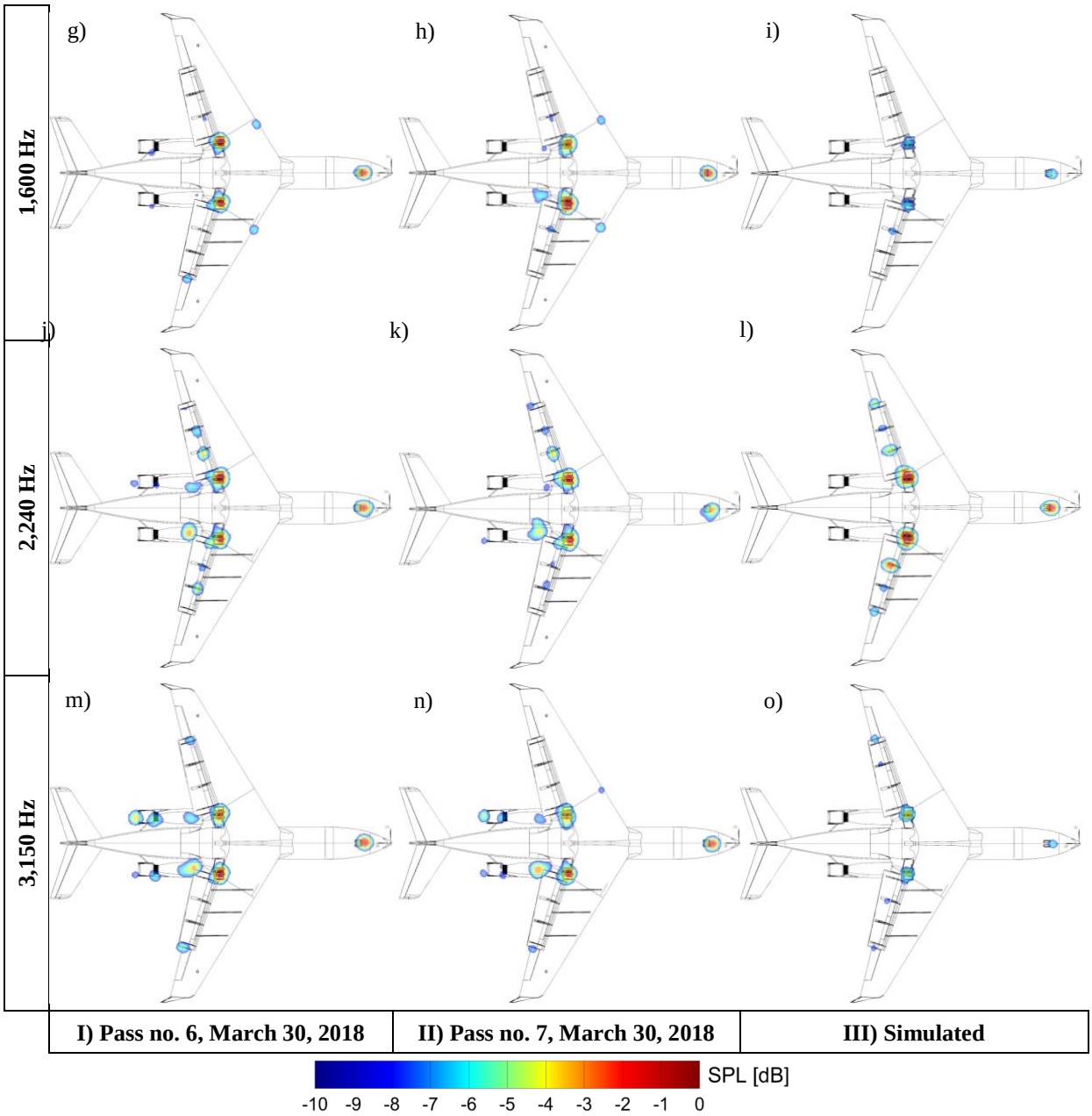

Fig. 5 Concluded.

a. Effect of Main Landing Gear Fairings

Sample maps for a flap deflection of 20° and main gear fairings installed are shown in Fig. 6 for frequencies of 1,120 Hz and 3,150 Hz. For this configuration, maps from three flyover passes with similar aircraft conditions and the corresponding synthetic map are displayed. The measured maps at 1,120 Hz (Figs. 6a-6c) demonstrate 2–3 dB reduction in the peak levels associated with the treated MLG when compared to the corresponding maps (Figs. 5d-5e) for the baseline gear. The map generated from simulated data (Fig. 6d) shows trends similar to those observed in the flight test data. However, upon comparison to the map with untreated gear fairings (Fig. 5f), a slightly higher reduction of the peak levels (approaching 3–4 dB) relative to the measured value was observed. The effectiveness of the fairings extends to higher frequencies, where larger reductions are observed when comparing the peak levels in Figs. 6e-6h to the maps for the untreated gear shown in Figs. 5m-5o. Again, the simulation predicted a larger reduction.

2. Landing Configuration

Beamform maps for the baseline case of flaps deflected at 39° and gear deployed (landing configuration) are shown next. At this higher deflection, flap noise produced at the inboard and outboard tips is a major source comparable to the landing gear component. Maps generated from measured and simulated pressure records are shown in Fig. 7 for frequencies of 425 Hz, 800 Hz, 1,120 Hz, 2,650 Hz, and 4,500 Hz. At the low frequency of 425 Hz (Figs. 7a-7d), the inboard flap tips emerge as the primary source, followed closely by the sources associated with the MLG. The map obtained from the synthetic data (Fig. 7d) captures, rather well, the emergence of inboard tip noise and its strength relative to other sources. However, at frequencies between 600 Hz and 900 Hz, the simulation overpredicted the peak levels associated with the flap inboard tips by 2–3 dB in comparison with the measurements. The maps at 800 Hz, shown in Figs. 7e-7h, clearly highlight this difference in peak values. Overprediction of the inboard tip noise extends to higher frequencies. The underlying cause of this behavior is not clear, but geometric fidelity may have contributed to the discrepancy. The G-III flap inboard and outboard tip geometries include a shallow cavity 0.5" (1.25 cm) deep that begins at the leading edge and extends over most of the flap chord. For obvious reasons, the cavity walls and lips are represented by sharp (90°) edges/corners in our digital aircraft model and are certainly different than what manufacturing tolerances allow. We speculate that the elevated noise levels may be attributed to the separated shear layer from the bottom edge of the cavity impinging on the sharp edge at the top, resulting in production and scattering of high-amplitude noise. The more rounded corners and other imperfections in the actual cavities may slightly alter this noise source. At the moderate frequency of 1,120 Hz, the maps produced from measured data (Figs. 7i-7k) show prominent sources located at the inboard tips, MLG, and NLG. There are noticeable variations in the relative strengths of these sources within the measured maps being compared. However, as discussed in Ref. [10], such differences in peak levels fall within pass-to-pass and day-to-day repeatability of the measured data. Also, around this frequency, the noise produced at the flap outboard tips gains prominence and begins to appear in the maps. The simulation (Fig. 7l) captures the same sources, albeit with the inboard tips being much stronger sources than the MLG, NLG, or outboard flap tips. At a higher frequency of 2,650 Hz (Figs. 7m-7o), the measured maps depict the outboard tips as the dominant noise source, with peak levels that are several dB above other sources. The map generated from the simulated data (Fig. 7p) accurately predicts the prominence of the outboard tip source. But, as alluded to earlier, the computation also overpredicted the noise being generated at the inboard flap tips. At a higher frequency of 4,500 Hz, both measured (Figs. 7q-7s) and simulated (Fig. 7t) maps are in very good agreement qualitatively and quantitatively, showing that the peak noise levels generated at the flap outboard tips are approximately 6 dB higher than any other airframe noise source.

a. Effect of Main Landing Gear Fairings

Sample beamform maps for the landing configuration (flap deflected 39°) with gear fairings installed are shown in Fig. 8 for a frequency of 2,650 Hz. As indicated previously, at this higher flap angle, the full extent of noise reduction achieved from application of the gear fairings is masked by flap inboard tip noise. Nonetheless, a comparison of the maps in Fig. 8 with those for the baseline gear shown in Figs. 7m-7p indicates that the acoustic treatments indeed reduced the peak levels associated with the main gear.

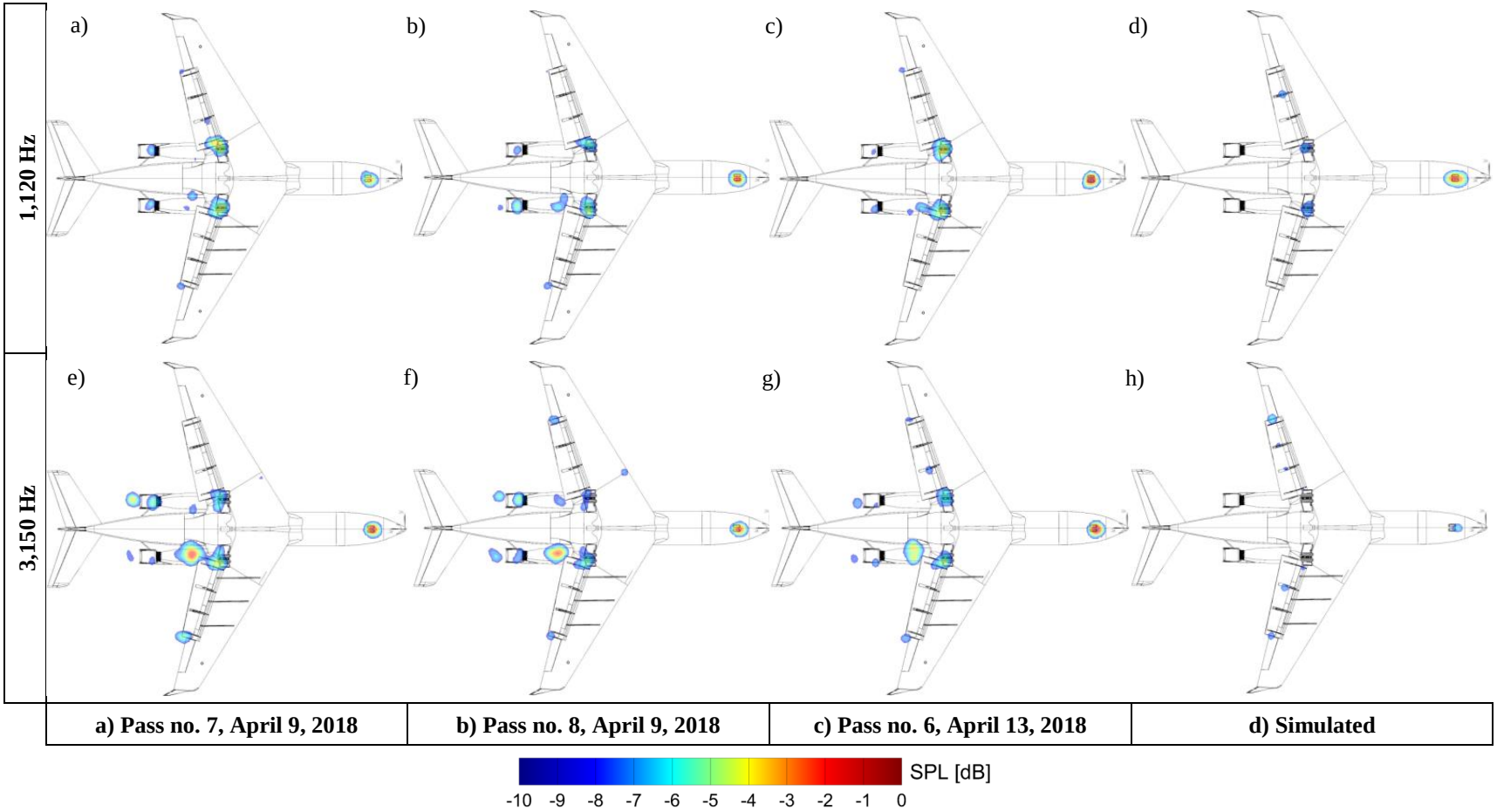

Fig. 6. Beamform maps for the 804 aircraft in landing configuration with flaps deflected 20°, landing gear deployed, and fairings installed; overhead position.

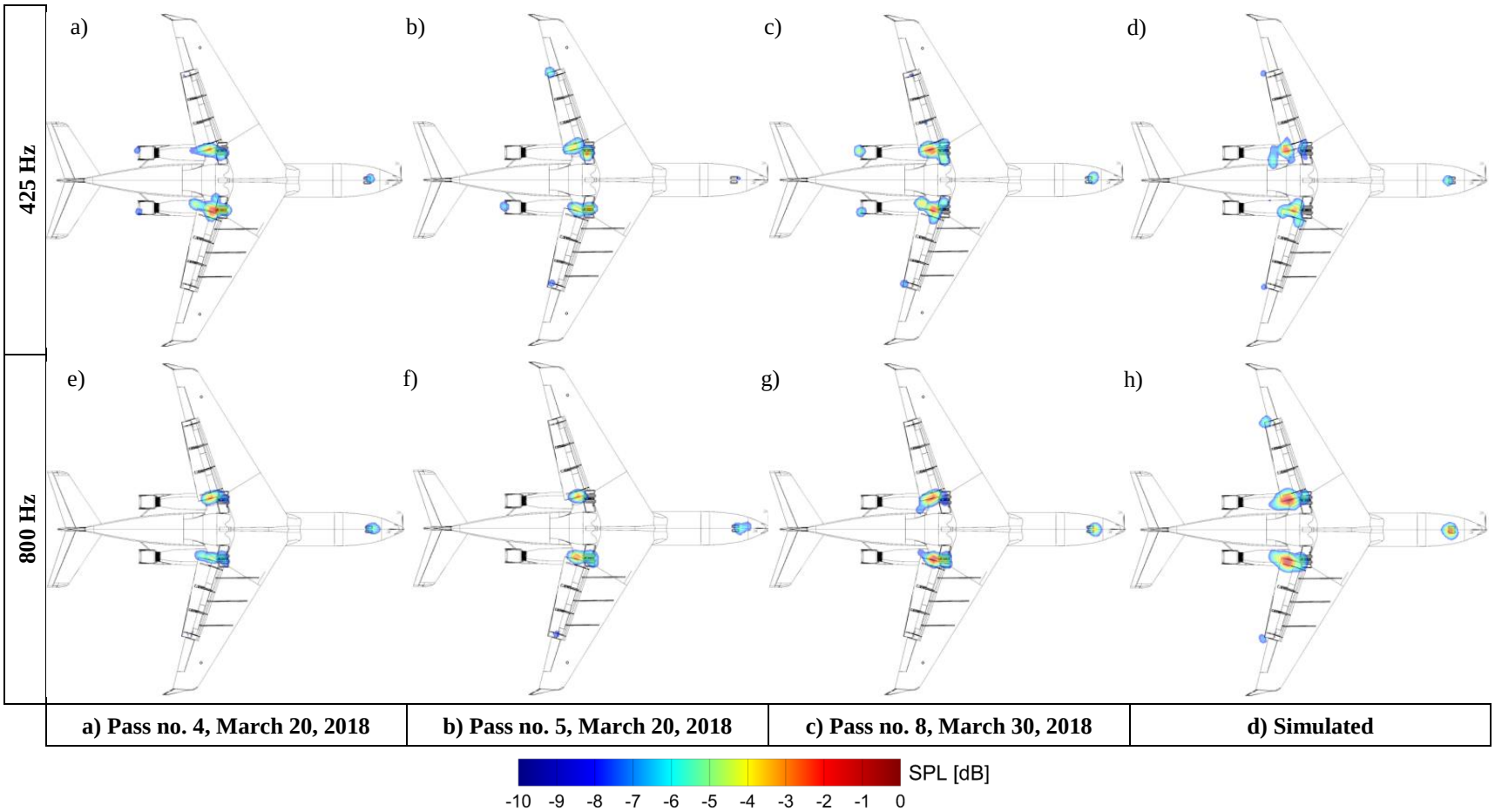

Fig. 7. Beamform maps for the 804 aircraft in landing configuration with flaps deflected 39° and landing gear deployed, overhead position.

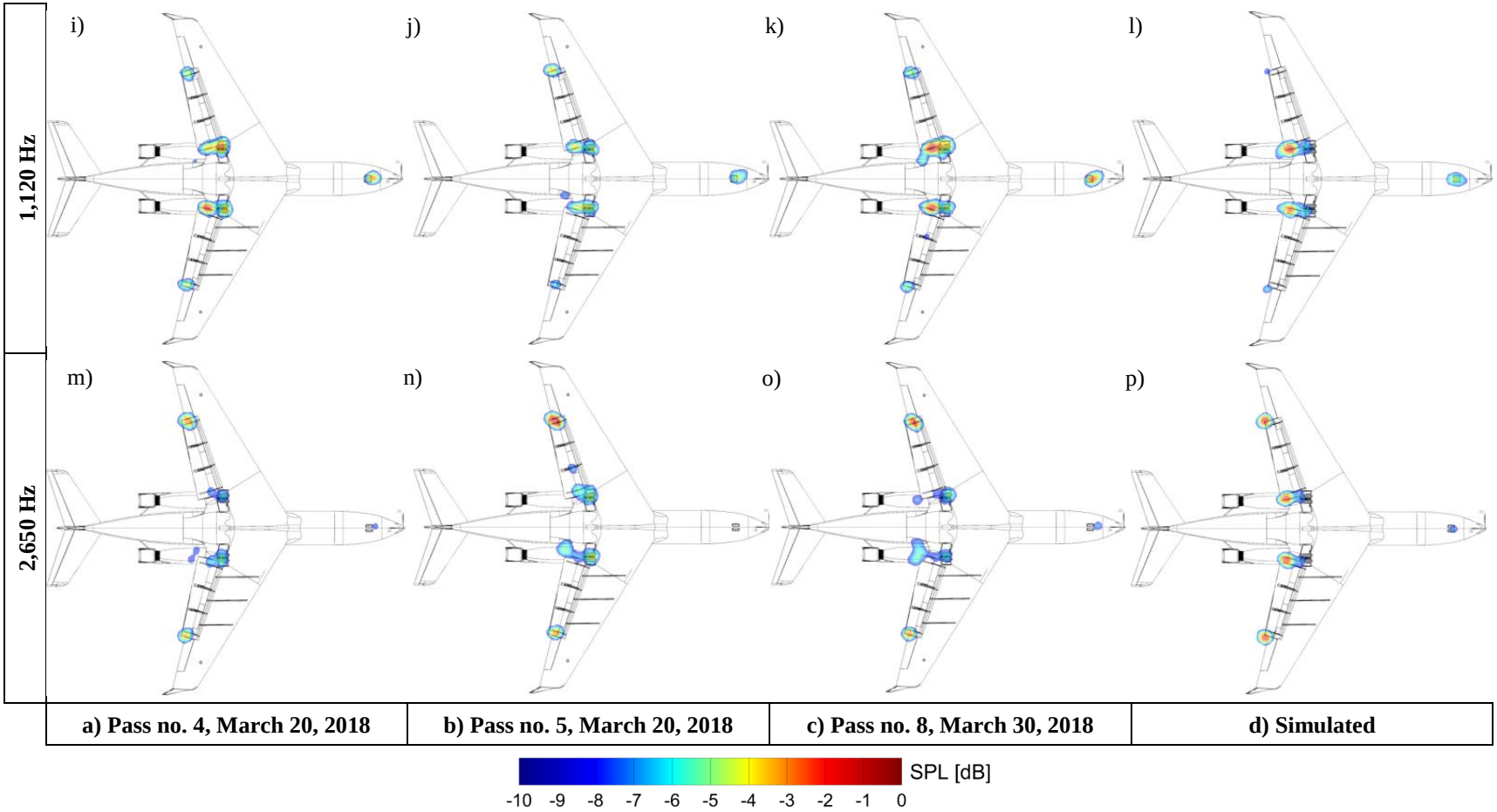

Fig. 7 Continued.

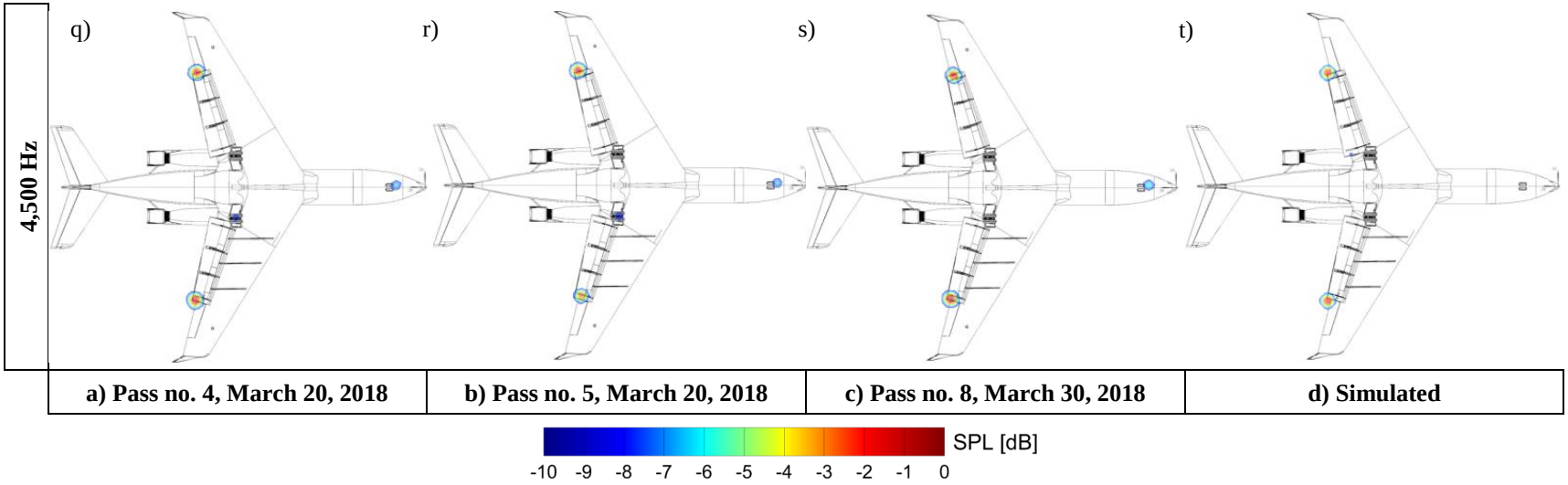

Fig. 7 Concluded.

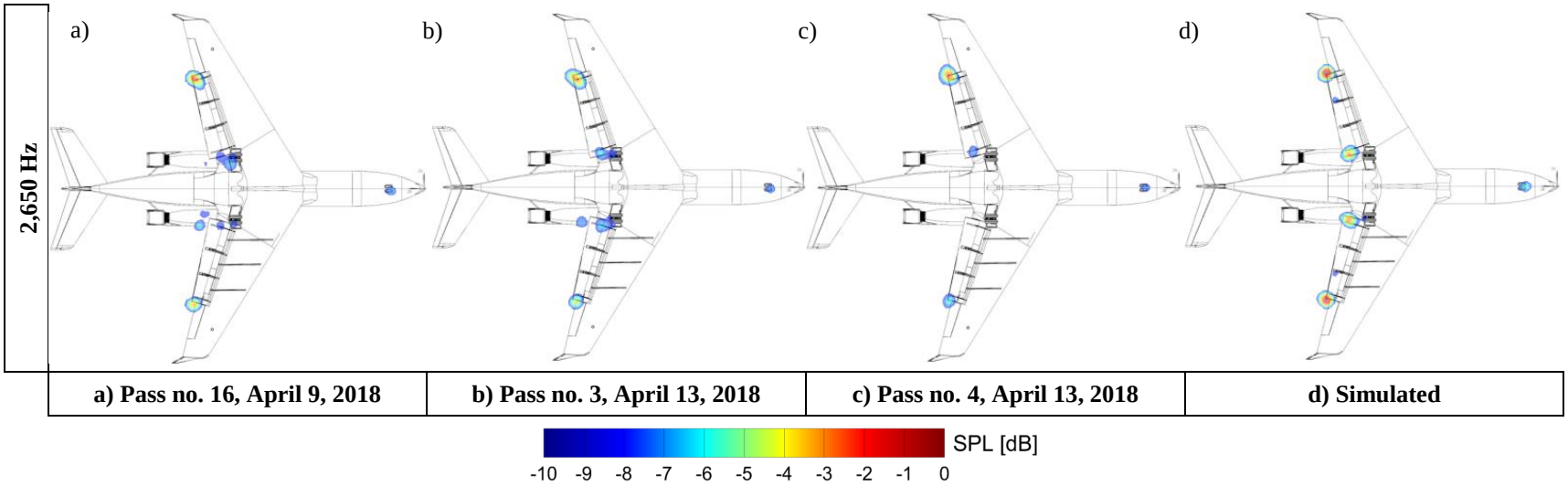

Fig. 8. Beamform maps for the 804 aircraft in landing configuration with flaps deflected 39°, landing gear deployed, and fairings installed; overhead position.

B. Integrated Farfield Spectra

Integrated farfield spectra help us to discern important trends in the radiated sound field across a broad frequency range for all configurations investigated. Two issues are worth examining before we compare simulated farfield acoustic behavior to that measured during the ARM-III flight test. The first issue is accuracy of the synthetic data, which were obtained from medium-resolution simulations. We planned to assess how much they differ from corresponding fine-resolution simulations, had the latter been completed on time as originally planned. Instead, previous fine-resolution simulations of slightly different configurations will be used. The second issue is addition of the NLG and whether the current simulations correctly capture the relative strength of this component and duplicate the trends observed in the measured data.

Spatial resolution effects and their impact on accuracy of the integrated farfield noise spectrum can be ascertained by comparing the current predicted results with those obtained from our previous fine-resolution simulations that exclude the NLG [13]. This is possible because the wake from the NLG has a minimal impact on development of the flow associated with the MLG or the flap [7]. "WingsNg"-based integrated spectra from current and past (Ref. [13]) simulations are shown in Fig. 9 for Fowler flaps deflected 20° with gear deployed (Fig. 9a) and ACTE flap deflected 25° with gear deployed (Fig. 9b). Due to the unavailability of acoustic data for the baseline 804 aircraft, only 808 aircraft acoustic measurements from the ARM-I (2016) and ARM-II (2017) tests were used to benchmark the computations of Ref. [13]. Thus, in addition to averaged[6] data from the ARM-III (2018) test, we included in Fig. 9a the spectrum obtained from averaging all the 808 passes. Differences in engine noise caused minor differences in the acoustic signatures from the two aircraft. Higher residual engine noise associated with the 804 aircraft is apparent in the frequency ranges 1,000 Hz < f < 2,000 Hz and f > 3,000 Hz. Also note from Fig. 9a that the spectrum from our previous fine-resolution simulation (without NLG) is in excellent agreement with the broadband component of the 808-averaged spectrum, precisely because of the lower engine noise emission of this aircraft. The medium-resolution spectrum (with NLG included) closely tracks fine-resolution levels up to a frequency of about 1,800 Hz; at higher frequencies, insufficient spatial resolution causes gradual degradation of the predicted noise levels. Despite this underprediction, the medium-resolution simulations produce the correct spectral trends and levels. As such, they can be used to determine the relative noise levels between baseline and treated configurations.

Similar observations regarding spatial resolution effects can be made when spectral results for the configuration with ACTE flaps deflected 25° and MLG fairings installed are compared (Fig. 9b). Since application of ACTE technology virtually eliminates flap noise (Refs. [8] and [13]), the differences between the two simulated spectra are mostly related to spatial resolution effects on the pressure field of the treated MLG. Although underprediction of the spectral levels begins modestly around 1,000 Hz, the current medium-resolution results track the fine-resolution spectrum and captures its overall trends and character up to a frequency of about 3,000 Hz.

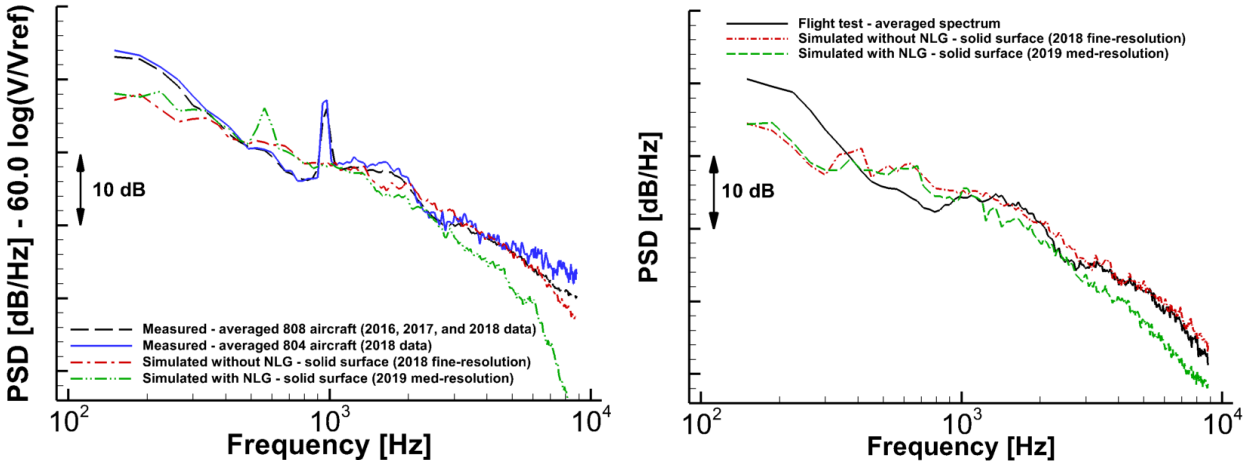

a) 20° Fowler flap deflection ("WingsNg" integration) **b) 25° ACTE flap deflection ("MLG" integration)**

Fig. 9 Integrated farfield spectra at overhead for G-III with Fowler and ACTE flaps. Fowler flap results are without gear fairings and ACTE flap results are with gear fairings installed.

[6] Averaged spectra were obtained using p^2 averaging.

To assess the strength of the NLG sources relative to those generated by the MLG, measured integrated spectra obtained from the "MLG" and "NG" regions for the configuration with Fowler flaps deflected 20° are plotted in Fig. 10a. For frequencies above 300 Hz, the NLG spectral levels are generally about 5 dB below MLG levels over a wide frequency range. The corresponding simulated spectra are shown in Fig. 10b. Similarly, a 5 dB offset in levels was predicted by the simulation. These results reaffirm our earlier claim that, while the absolute values may be underpredicted by the current medium-resolution simulations, the relative levels are well predicted.

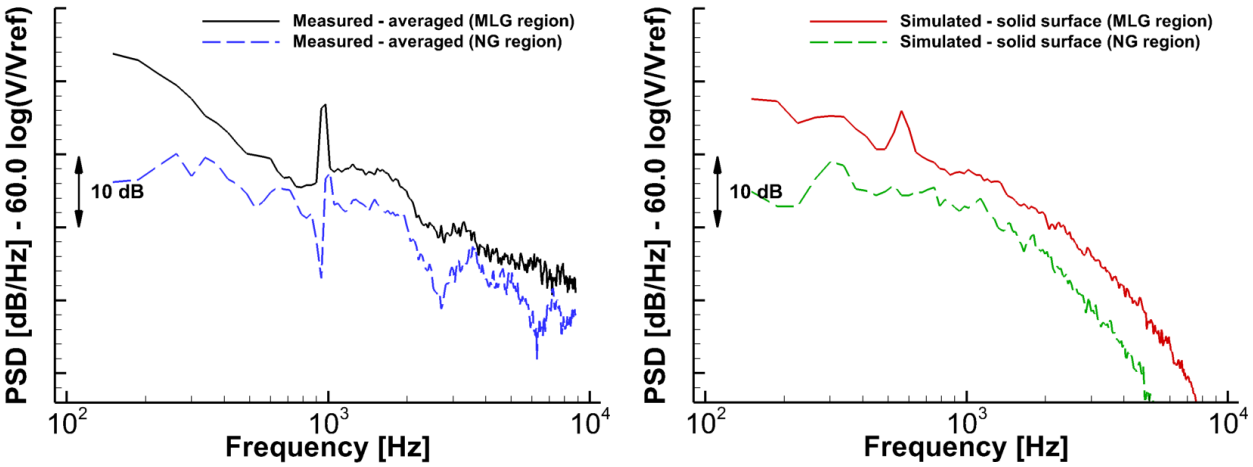

a) Measured **b) Simulated**

Fig. 10 Integrated farfield spectra from "MLG" and "NG" regions at overhead for G-III with Fowler flaps deflected 20° and landing gear deployed.

1. Approach Configuration

The integrated spectra obtained from the "WingsNG", "MLG", and "NG" regions are presented in Figs. 11a-11c for the baseline case of flaps deflected 20° and landing gear deployed. Recall that the noise from the landing gear is the dominant component at this flap deflection. Included in the figure are spectra from individual aircraft passes, their average (based on p^2 averaging), and the predicted spectra obtained from pressures collected on the aircraft surface and on a permeable FWH surface (see Fig. 3).

Measured spectra from the "WingsNg" region (Fig. 11a) show that the peak levels occur at frequencies below 400 Hz. These levels result from a combination of MLG cavity noise and fuel vapor vent tones that are scattered by the aircraft surfaces within the integration region (see Ref. [8]). The strong tone in the 900 Hz – 1,050 Hz range is generated by the hollowed front post of the MLG at the knee joint. The simulated spectrum obtained from solid surface pressures captured the overall character of the measured spectrum rather well, with the tonal noise generated by the MLG knee joint present in the 500 Hz – 600 Hz frequency range. As explained in Ref. [13], this disparity in the tonal frequency was caused by differences in the internal shape and dimensions of the hollowed post, which had to be estimated because they could not be discerned from the laser scans of the full-scale gear. The simulated spectrum underpredicts the measured levels in the frequency bands $f < 400$ Hz, 1,200 Hz $< f <$ 2,000 Hz, and $f >$ 3,000 Hz. The discrepancies in the lower band are attributed to the poor geometric fidelity of the simulated MLG cavity and the absence of fuel vapor vents in our simulations. The differences between measured and simulated spectra at moderate and high frequencies are partly caused by excess residual engine noise of the 804 aircraft and by insufficient spatial resolution in our simulation. The spectrum obtained from permeable surface data matches the solid surface result up to a frequency of 1,000 Hz. Beyond this frequency, however, it deviates rapidly with a faster roll-off. This deviation and accelerated roll-off are likely caused by excessive diffusion of mid- and high-frequency waves as they convect toward the permeable surface where the data were collected [13].

The spectra obtained from integration of the "MLG" region (Fig. 11b) are very similar in character to those from the "WingsNg" zone, corroborating the dominance of landing gear noise at the 20° flap deflection. The relatively larger divergence between measured and solid surface-simulated levels at frequencies above 3,000 Hz is caused by exclusion of flap outboard tip noise from the integration. Notice that exclusion of the outboard tip sources does not result in noticeable differences in measured spectral levels between the two integration regions. This is due to engine noise contamination at higher frequencies, which is included in the integration regions and masks the contribution from sources at the outboard tips.

The farfield noise footprint of the NLG obtained from integration of the "NG" region is shown in Fig. 11c. The measured spectra reveal a very gradual change in noise levels at frequencies below 2,000 Hz. The rapid drop in level at 950 Hz is caused by the MLG knee joint tone and the array signal-to-noise ratio (SNR) – since this tone is the dominant source by over 10 dB, no other sources could be accurately integrated at this frequency. For reasons not well understood yet, the measured spectra also show a significant dip in noise levels at frequencies 2,300 Hz < f < 3,000 Hz. The simulated spectrum based on solid surface data agrees well with measurements, both in shape and magnitude, for frequencies up to 3,000 Hz. Notice also that there is much better agreement between the synthetic spectra obtained from solid and permeable surfaces. This effect results mainly from the isolated nature of the nose landing gear, which permitted placement of the permeable surface closer to the gear when compared with the MLG or flap components.

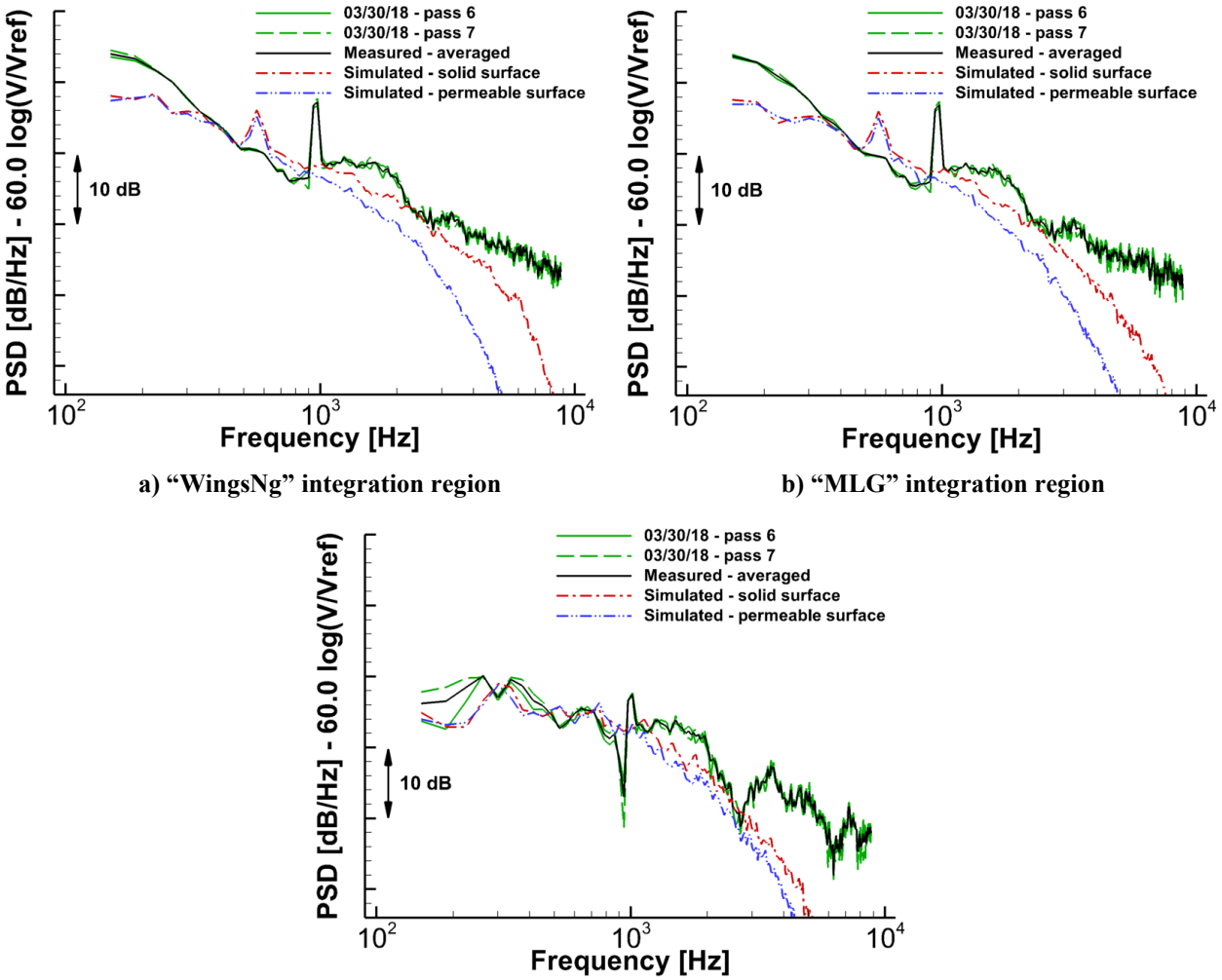

a) "WingsNg" integration region

b) "MLG" integration region

c) "NG" integration region

Fig. 11 Integrated farfield spectra at overhead for G-III with Fowler flaps deflected 20° and landing gear deployed.

Farfield spectra obtained from the three integration zones for the configuration with Fowler flaps at 20° and MLG fairings installed, are displayed in Figs. 12a-12c. For comparison purposes, only the simulated spectrum obtained from solid surface pressures[7] and an average from measured spectra are plotted. Note from the figures that both measured and predicted spectra when the gear fairings were installed display a behavior similar to that observed for the

[7] Spectra obtained from permeable FWH surface data underpredict the spectral levels in a manner similar to that presented in Figs. 11a – 11c. Therefore, they were excluded from this and all subsequent comparisons.

configuration without fairings (Fig. 11a-11c). We emphasize that underprediction of the spectral levels at moderate and high frequencies is partially due to inadequate spatial resolution and partially to higher engine noise for the 804 aircraft. Notice also from Fig. 12 that both measured and simulated spectra indicate that the fairings eliminate the prominent tone generated by the MLG knee joint.

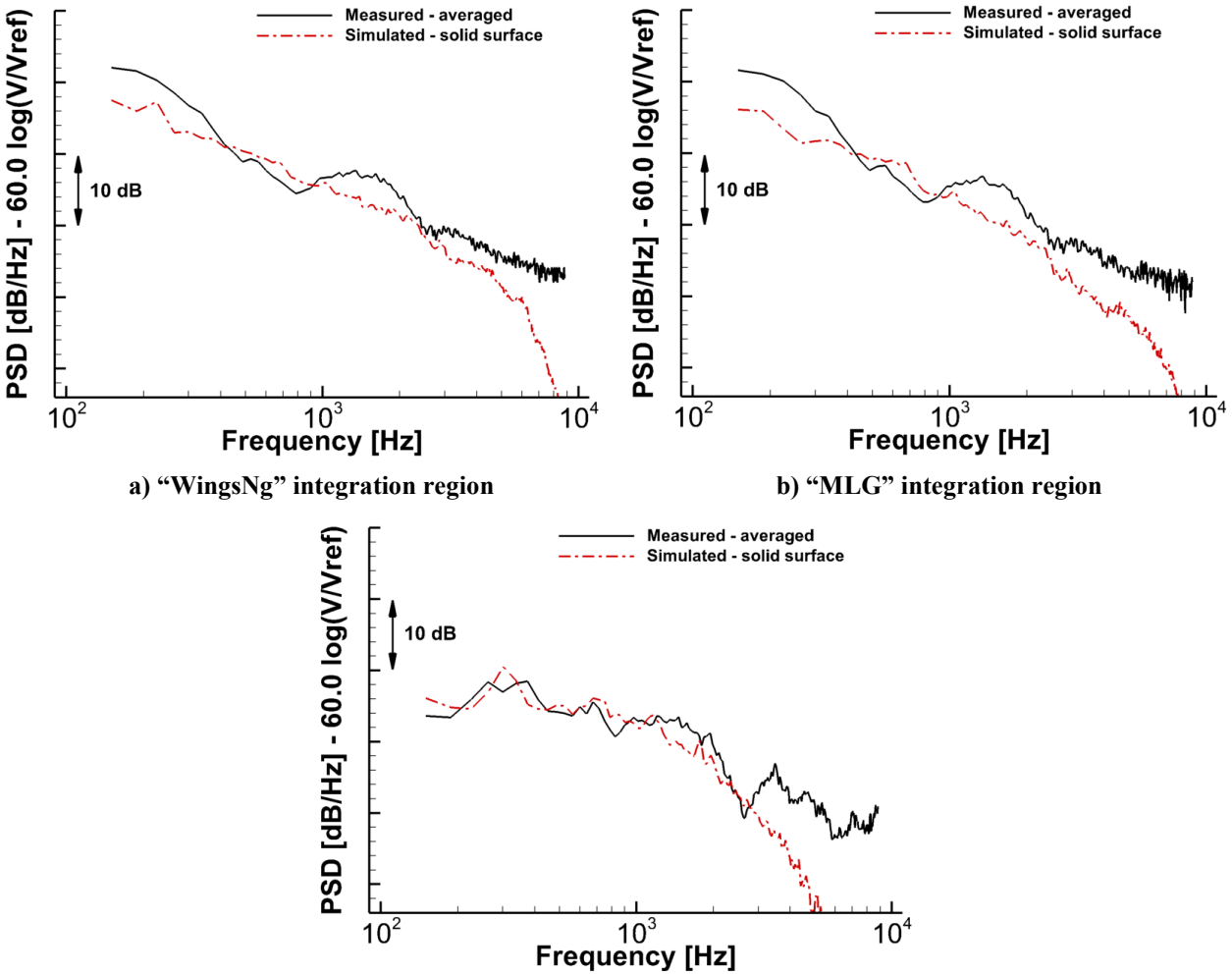

a) "WingsNg" integration region

b) "MLG" integration region

c) "NG" integration region

Fig. 12 Integrated farfield spectra at overhead for G-III with Fowler flaps deflected 20° and landing gear fairings installed.

2. Landing Configuration

Integrated farfield spectra for the configurations with Fowler flaps deflected 39° without and with MLG fairings installed are shown in Figs. 13 and 14, respectively. Notice that, relative to those of Figs. 11a and 11b, the solid-surface-based predicted spectra from "WingsNg" (Figs. 13a and 14a) and "MLG" (Figs. 13b and 14b) regions are in much better agreement with measured data at frequencies above 2,500 Hz. Because of the higher noise levels produced at the flap tips at this larger deflection angle, particularly the outboard tip, the 804 residual engine noise contribution to the farfield spectrum at higher frequencies is not as dominant as in the case of the 20° flap deflection. As we saw in the beamform maps, the simulations properly capture the noise from the flap tips and hence produce better agreement with flight test data. We also note the presence of a broad tonal hump in the simulated spectra (Figs. 13a and 14a) in the frequency range 5,000 Hz < f < 6,000 Hz. As mentioned in section IIIA, we attribute this tonal feature to the presence of a shallow cavity at the outboard tip. Figures 13a and 14a also indicate the presence of a similar feature in the measured spectra. The predicted spectrum obtained from the "MLG" region (Fig. 13b) also agrees well with measurements over a wide frequency range. Even better agreement is attained when the MLG fairings are installed (Fig. 14b). Integration of the "NG" region produces spectra (Figs. 13c and 14c) that are very similar to

those presented for the 20º flap deflection (Fig. 12b). This outcome was anticipated, since the NLG resides at the front of the aircraft, isolated from any other component, and thus its noise signature remains unmodified.

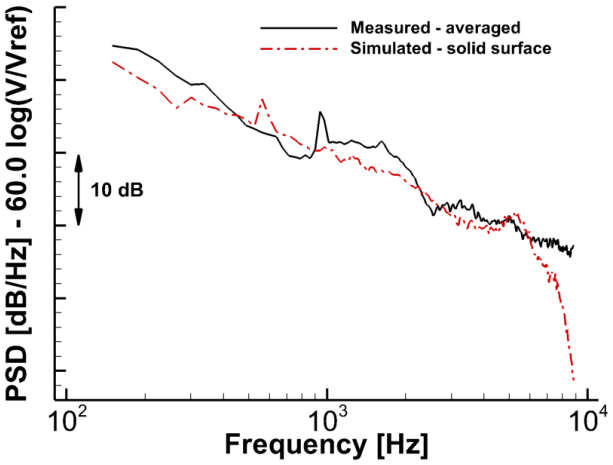

a) "WingsNg" integration region

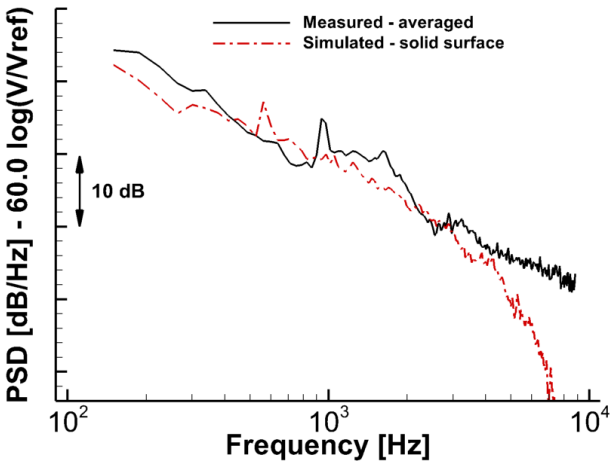

b) "MLG" integration region

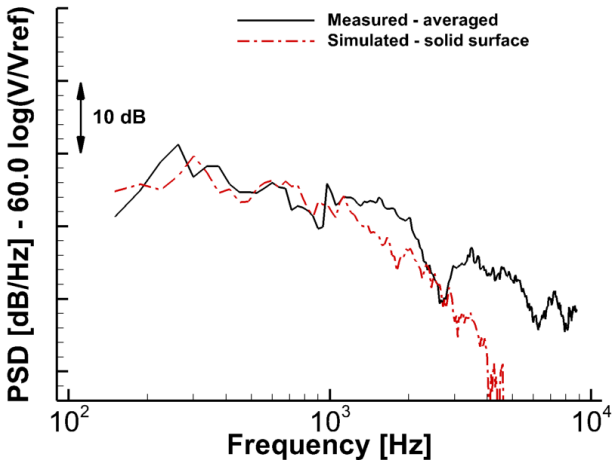

b) "NG" integration region

Fig. 13 Integrated farfield spectra at overhead for G-III with Fowler flaps deflected 39° and landing gear deployed.

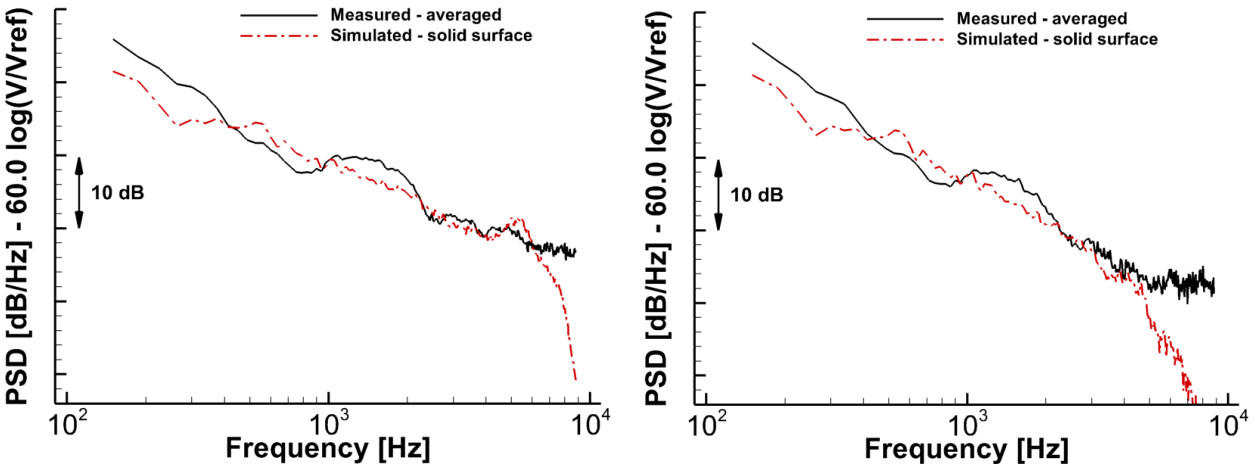

a) "WingsNg" integration region

b) "MLG" integration region

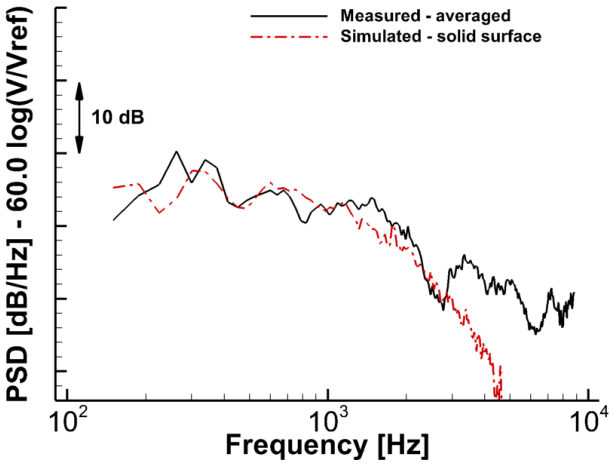

b) "NG" integration region

Fig. 14 Integrated farfield spectra at overhead for G-III with Fowler flaps deflected 39° and landing gear fairings installed.

3. Acoustic Performance of Main Landing Gear Fairings

The noise reduction performance of the MLG fairings for an aircraft equipped with conventional Fowler flaps was determined by subtracting the spectral levels for the configurations with treated gear from the corresponding levels for the configurations with untreated (baseline) gear. Measured and predicted noise reduction levels for flap deflections of 20° and 39°, are shown in Figs. 15a and 15b, respectively. The integrated spectra were obtained from the "MLG" region. At the lower flap deflection (Fig. 15a), the predicted results show reduction levels on the order of 3 to 4 dB, which are maintained over a wide frequency range approaching 4,000 Hz. Beyond this frequency, the accuracy of the simulated results is questionable due to insufficient spatial resolution. The measured values indicate reduction levels approaching 2 to 3 dB. The lower noise reduction obtained from the measurements was anticipated since, as we noted earlier, the true acoustic performance of the fairings was masked by residual engine noise. The much larger reductions that appear as narrow band peaks at frequencies of 550 Hz (simulated) and 950 Hz (measured) resulted from elimination of the MLG knee joint tone when the fairings were installed. Better agreement between predicted and measured noise reduction levels was achieved at the higher (39°) flap deflection, as seen in Fig. 15b – a 2 dB reduction in farfield noise levels that is maintained for frequencies up to 3,000 Hz. In reality, however, we anticipate the reduction in gear noise to be much higher. The underprediction in acoustic performance of the fairings is caused by the extreme difficulty of isolating contributions from the MLG and flap inboard tip noise sources when they are in very close proximity of each other and are inevitably contained within the same ("MLG") integration zone. Observe also in Fig. 15b that the measured values show much higher reduction levels at frequencies above 3,000 Hz.

Unfortunately, inadequate spatial resolution of the flow field surrounding the MLG porous fairings resulted in underprediction of the high-frequency content of the farfield spectrum.

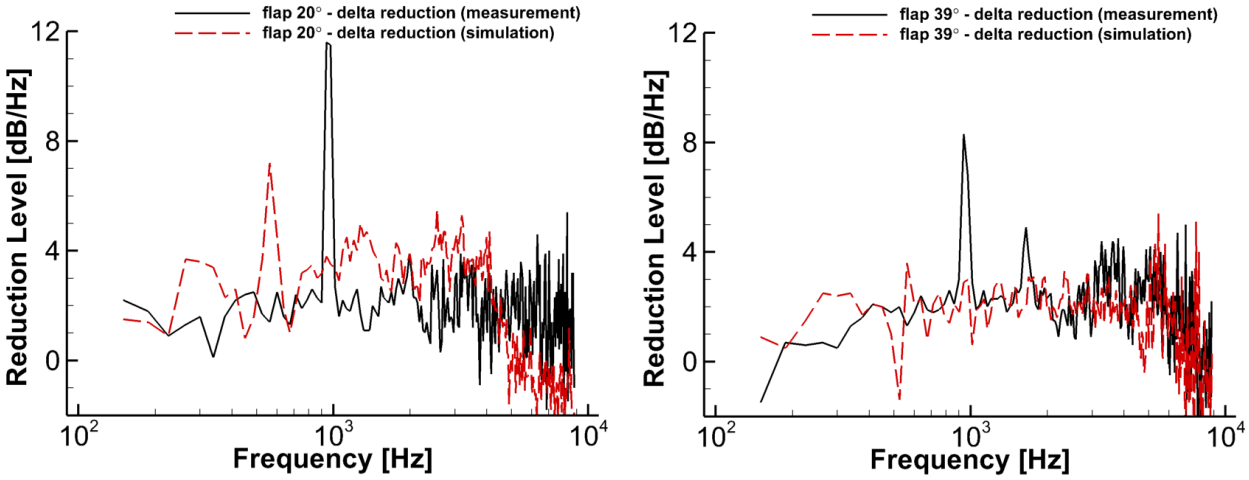

a) 20° flap deflection **b) 39° flap deflection**

Fig. 15 Noise reduction levels achieved with MLG fairings at overhead for G-III with Fowler flaps. Results obtained from integration of "MLG" region.

C. Effective Perceived Noise Level

Of paramount importance to the aerospace industry is the EPNL metric used for aircraft noise certification. Generation of EPNL data with relatively low uncertainty levels from the pole-mounted microphone measurements of ARM tests is a complex endeavor fraught with many challenging issues that could affect the end results. For example, the frequency content and amplitude of the background noise at the test site plays a critical role in the quality of the measured acoustic information by setting the SNR during data acquisition and thus affecting the number of flyover passes deemed acceptable for EPNL calculations. The focus of the ARM tests was to acquire phased array measurements; collection of single microphone data was a lower priority. Thus, a low background noise environment that would be ideal for aircraft certification was not the sole driving factor during selection of the test site. As mentioned in Ref. [12], the background noise levels at the Edwards Air Force Base, where the ARM tests were conducted, were somewhat higher than desired for acquisition of certification microphone data. As a result, the EPNLs generated from the ARM tests may have relatively high uncertainties associated with them [12]. Also important are the local meteorological conditions encountered during the testing period, which could greatly impact the attenuation of sound waves in the mid- to high-frequency ranges and thus set the magnitude of the amplitude corrections that have to be imposed on the gathered data.

To the best of our knowledge, this is the first time that a comparison of synthetic EPNL values with flight test measurements has been attempted. Thus, the exercise should be viewed as an exploratory, qualitative analysis to determine if the predicted trends follow those observed from flight tests. Achievement of a reasonably accurate prediction of EPNL is an arduous task that requires consideration of many additional factors that affect both measurements and simulations and are beyond the scope of the present study. Among these factors is availability of accurate synthetic data at high frequencies, since EPNL calculation requires spectral contents for frequencies over 12 kHz. As shown earlier, medium-resolution simulation results show a rapid roll-off for frequencies beyond 5 kHz that would likely impact the EPNL levels. All simulated EPNL data presented in this section were obtained using the pressures collected on the solid airframe surfaces. To eliminate potential sources of discrepancy, the contributions from a 270 Hz trapped mode in the NLG cavity (see Ref. [7]) and a 550 Hz tone associated with the MLG knee joint were removed from the simulated pressure records prior to computing PNL values.

Sample simulated tone-corrected Perceived Noise Level (PNLT) results for the configuration with Fowler flaps deflected 39º and landing gear deployed are shown in Fig. 16 for two glide slopes: 7° and 3°, the latter being required by ICAO [18] and FAA [19] certification rules. Comparison of the curves obtained with the as-flown slope and the recommended slope reveals that a variation of a few degrees in the glide slope has only a minor effect on the level or character of the perceived noise as the aircraft flies by. Integration of the PNLT curves over the 10 dB-down period produced EPNL values that only differ by about 0.1 EPNdB, corroborating the insensitivity to the glide slope of pole-

mounted microphone and phased array results from ARM tests presented in Refs. [10] and [12]. Based on the spatial resolution study of Ref. [6] for a configuration without NLG, except for modest increases in levels near $PNLT_{max}$, we anticipate that the trends observed in Fig. 16 to hold with increased spatial resolution.

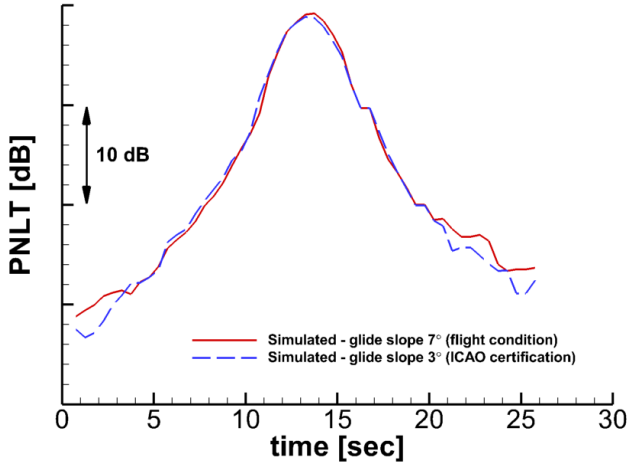

Fig. 16 Effect of glide slope on the PNLT time history of a G-III with Fowler flaps deflected 39° and MLG/NLG deployed (landing configuration).

Sample plots of predicted PNLT levels and measurements for select passes with similar aircraft conditions for the baseline configurations of Fowler flaps deflected 20° and 39° with gear deployed are shown in Fig. 17. Measurements from two pole-mounted certification microphones in the flyover direction (called Flyover 1 and Flyover 2) are included in the figure. During the ARM tests, Flyover 1 was positioned 100 m upstream of the microphone phased array center and Flyover 2 was placed 100 m downstream of the array center. For comparison purposes, the simulated curves were time-shifted so that their $PNLT_{max}$ align with corresponding measured values. The synthetic PNLT for a flap deflection of 20° (Fig. 17a) are in remarkable agreement with measured values in the segment within 10 dB down from the peak. In contrast to predicted levels, the measured PNLT values show a more gradual rise in noise prior to $PNLT_{max}$. This behavior was expected, as it results from engine noise and various other secondary sources on the aircraft that were not included in the simulation. The results for a flap deflection of 39° (Fig. 17b) also depict good agreement between simulated and measured PNLT curves. At this higher flap deflection, however, the simulation produced a $PNLT_{max}$ that is 2–3 EPNdB higher than the measured value. We partially attribute this discrepancy to overprediction of noise from the flap inboard and outboard tips, mentioned previously in section III.A. As observed for the lower flap deflection, the measurements show a more gradual rise of the PNLT values relative to the computed levels as the aircraft approaches an observer on the ground. Although a reasonable agreement between simulated and measured PNLT values was expected (based on the accuracy of the integrated farfield spectra demonstrated in our previous [13] and present studies), we did not anticipate that the simulations would so closely track the flight test trends and produce such good agreement within 10 dB down from the peak. This agreement is even more remarkable given the host of factors that could profoundly affect the quality, consistency, and accuracy of the measured PNLT values (see Ref. [12]).

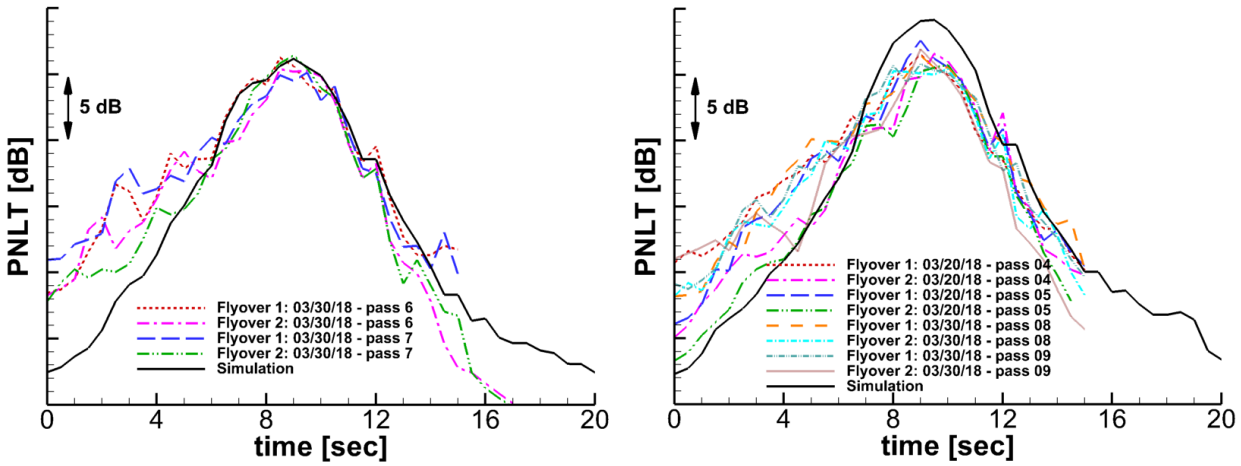

a) Fowler flap 20° gear deployed (approach) **b) Fowler flap 39° gear deployed (landing)**

Fig. 17 Comparison of simulated and measured PNLT time histories for G-III on approach and landing conditions.

1. Effect of Airframe Noise Reduction Technologies

Acoustic data for baseline configurations involving the 808 aircraft are available from all three ARM tests, while similar data for 804 are only available from ARM-III (2018). Therefore, for configurations with the ACTE flap, which were tested on 804 during ARM-II (2017), we will use 808 baseline data obtained during 2017 as well as 804 baseline measurements acquired during the 2018 test campaign. Since farfield noise is insensitive to variations in glide slope and AOA [10, 12], rather than restrict our analysis to a few select passes we have chosen to use the p^2-based averages of all acceptable passes for each configuration of interest to obtain the EPNL data used in this section.

Noise reductions attained for the configuration with ACTE flaps deflected 25° and MLG fairings installed, relative to the baseline configuration of Fowler flaps deflected 20° and MLG/NLG deployed, are presented in Table 2. These two configurations, which represent the G-III aircraft during approach, have similar aerodynamic performance. For measured values, we also include the 90% confidence interval as stipulated in the noise certification standard [19]. Applying the ACTE flap and MLG fairings resulted in a predicted noise reduction in excess of 4.5 EPNdB. The measured reduction was approximately 2.3 EPNdB, which is more than 2 EPNdB smaller than the predicted value. Overprediction of simulated noise reductions is to be expected for any such comparison due to the presence of engine noise and other secondary sources on the aircraft that increase the noise floor in the measurements (see Ref. [8]) and mask the true performance of the noise reduction technologies.

Table 2. EPNL reduction relative to baseline configuration with Fowler flaps deflected 20° and gear deployed.

Microphone	Simulation ACTE 25° with Fairings	Experiment ACTE 25° with Fairings relative to 808 (2017)	Experiment ACTE 25° with Fairings relative to 804 (2018)
Flyover 1	4.6	2.39 ± 0.49	1.85 ± 0.59
Flyover 2		2.71 ± 0.37	

The noise reductions for the configuration with ACTE flaps deflected 25° and MLG fairings installed, relative to the configuration with Fowler flaps deflected 39° and gear deployed, are listed in Table 3. As expected, a much larger noise reduction (≈ 7.0 EPNdB) was predicted because of higher baseline flap noise produced at this larger deflection angle. Since application of ACTE technology virtually eliminates flap noise [8, 13], the extra noise reduction mostly comes from mitigation of flap noise. In contrast, the values extracted from flight measurements show smaller reductions of approximately 2.75 EPNdB. The wide spread between predicted and measured acoustic benefits is directly related to the higher noise floor present in the measurements, making it virtually impossible to deduce the full extent of the noise reduction from the acquired acoustic data.

Table 3. EPNL reduction relative to baseline configuration with Fowler flaps deflected 39° and gear deployed.

Microphone	Simulation ACTE 25° with Fairings	Experiment ACTE 25° with Fairings relative to 808 (2017)	Experiment ACTE 25° with Fairings relative to 804 (2018)
Flyover 1	7.1	2.87 ± 0.50	2.38 ± 0.39
Flyover 2		3.02 ± 0.50	

We now examine the performance of the MLG fairings in conjunction with a Fowler flap system. Since these aircraft configurations were tested during ARM-III (2018), only 804 baseline data obtained during the same test campaign were used to determine the acoustic performance of the fairings. The differences in noise levels for the configuration with Fowler flaps deflected 20° without and with MLG fairings are presented in Table 4. Included in the table are measured noise reductions attained for the configuration with both MLG and NLG retracted. These values represent the upper bound of the noise reduction ceiling (gear-flap interaction alters the noise produced by both components) if the applied gear technologies were able to eliminate gear noise totally. Since noise treatments were installed only on the MLG, the achievable reduction would be less than the ideal upper bound. Note from Table 4 that the measured reduction due to application of the gear fairings falls somewhere between 1.3 and 1.4 EPNdB, which represents a substantial portion of the maximum possible reduction of approximately 3 EPNdB if both MLG and NLG were absent. The predicted reduction of about 1.2 EPNdB is slightly less than the measured values. Since the simulations are devoid of noise from engines or other secondary sources, we were expecting reduction levels that are much higher than measured values, as we observed in the ACTE results of Table 2. This discrepancy may have been caused by a) overprediction of flap tip noise and/or b) insufficient spatial resolution to capture high-frequency behavior associated with MLG noise.

Corresponding noise reductions for the higher flap deflection of 39° are given in Table 5. Because of higher and more erratic background noise at the test site during the 2018 ARM-III test [12] and the low number of passes executed for gear-up configurations, data measured for the configurations with flaps deflected 39° should be viewed with caution. As expected, because of higher noise levels produced by the flaps at this setting, the true acoustic performance of the MLG fairings cannot be determined. Predicted noise reduction for this flap deflection approaches 1.0 EPNdB, which is certainly higher than the approximately 0.3 EPNdB reduction extracted from the Flyover microphones. The larger reduction predicted by the simulation (relative to the experiments) at this flap setting reinforces our earlier assertion that the synthetic reduction obtained for the configuration with flaps deflected 20° is too low.

Table 4. EPNL reduction relative to baseline configuration with Fowler flaps deflected 20° and gear deployed. Experimental results relative to 804 baseline measurements obtained in 2018.

Microphone	Simulation Fowler 20° with Fairings	Experiment Fowler 20° with Fairings	Experiment Fowler 20° Gear Up
Flyover 1	1.17	1.40 ± 0.64	3.33 ± 0.61
Flyover 2		1.34 ± 0.62	2.74 ± 0.57

Table 5. EPNL reduction relative to baseline configuration with Fowler flaps deflected 39° and gear deployed. Experimental results relative to 804 baseline measurements obtained in 2018.

Microphone	Simulation Fowler 39° with Fairings	Experiment Fowler 39° with Fairings	Experiment Fowler 39° Gear Up
Flyover 1	0.97	0.39 ± 0.40	0.65 ± 0.66
Flyover 2		0.14 ± 0.44	0.58 ± 0.52

IV. Summary

A comparative acoustic analysis between high-fidelity, full-scale simulations and data acquired during the NASA ARM flight tests was presented in this paper. A select set of simulations that duplicated “as flown” aircraft conditions from the ARM-II (2017) and ARM-III (2018) tests was performed to benchmark the predictive capability of the lattice Boltzmann computational methodology in capturing the farfield noise signatures of a G-III aircraft with and without

airframe noise reduction technologies. The simulated configurations were the Fowler flap-equipped G-III, with and without main landing gear fairings, flown during the ARM-III test and the ACTE flap-equipped G-III flown during the ARM-II test. The comparison was extended to include aircraft certification metrics that are of great interest to the aerospace industry, such as PNLT and EPNL, by including a high-definition replica of the aircraft nose landing gear in the digital model. To ascertain the accuracy of the simulated results, simulations on coarse-, medium-, and fine-resolution grids were attempted. Due to unforeseen circumstances beyond our control, the fine-resolution simulations were not completed in time to be included in the present analysis. The effects of spatial resolution on the accuracy of predicted farfield spectra were assessed indirectly via comparison of fine-resolution simulations of configurations without the nose landing gear from a previous study with current predictions obtained on medium-resolution grids. The medium-resolution simulations produced results with sufficient accuracy to properly capture the farfield noise spectrum for frequencies approaching 3,000 Hz.

The simulated results were validated via source localization (beamform) maps, integrated farfield noise spectra, and PNLT/EPNL metrics. Data collected on the aircraft solid surfaces were used with a FWH formulation to obtain the time-dependent pressure records at the same phased-array and pole-mounted microphone locations used during flight tests. For consistency, both measured and synthetically generated phased-array pressure records were processed using the CLEAN approach. Simulated and measured pole-mounted microphone pressures were processed following ICAO procedures to generate PNLT time histories and EPNL values. Simulated and measured beamform maps for Fowler flap deflections of 20° and 39° with MLG and NLG deployed were in good agreement for frequencies up to 3,000 Hz. Both experimental and synthetic beamform maps indicated that the G-III NLG is a major noise source across a broad frequency range, producing noise levels that are slightly lower than those for either MLG. The strength of the sources at the flap tips were overpredicted in the simulated maps, exceeding measured levels by 2–3 dB in the 600 Hz – 900 Hz frequency range and at frequencies above 3,000 Hz. This overprediction is attributed to the idealized representation of the shallow cavities at both flap tips in the aircraft digital model.

Farfield spectra were obtained from integration of the simulated and measured maps within regions that either isolated or combined the contributions from the flaps, MLG, and NLG. Good agreement between predicted and measured integrated farfield spectra was demonstrated, in particular for 39° flap deflection, where contamination from residual engine noise is less significant. The noise reduction performance of the MLG fairings was determined by subtracting the noise levels of a treated gear configuration from those of the corresponding untreated gear configuration. The predicted noise reduction attained with the MLG fairings was in remarkable agreement with measured values, indicating reductions of 3–4 dB and 2 dB for Fowler flap deflections of 20° and 39°, respectively. However, determination of the full performance for the MLG fairings at the higher flap deflection was hampered by flap inboard tip sources present within the integration region.

Arguably the first of its kind, this investigation also showed that simulated PNLT time histories for the two baseline configurations with Fowler flaps deflected 20° and 39° and landing gear deployed were in very good agreement with measured data, predicting well the magnitude of $PNLT_{max}$ and the overall character of the sound signature as received by an observer on the ground. The predicted reduction in EPNL values due to installment of the ACTE technology and/or MLG fairings followed the trends observed in the measurements at all simulated flap deflections. Given the many factors that can affect measurement and processing of pole-mounted microphone data and the limited frequency range for which medium resolution simulations match the experiments, the observed agreement far exceeded our expectations and bodes well for future use of the current computational approach as an aid during the aircraft certification process.

Acknowledgments

This work was supported by the Flight Demonstrations and Capabilities project under the Integrated Aviation Systems Program of the NASA Aeronautics Research Mission Directorate. The flight tests results would have not been possible without the dedicated effort of a large group of people, especially the NASA AFRC personnel and the NASA Langley Research Center microphone array team. All simulations were performed on the Pleiades supercomputer at the NASA Advanced Supercomputing (NAS) facility at Ames Research Center. The logistical support provided by NAS staff is greatly appreciated.

References

[1] Dobrzynski, W., "Almost 40 Years of Airframe Noise Research: What Did We Achieve," *J. Aircraft*, Vol. 47, No. 2, March-April 2010, pp. 353–367.

[2] Khorrami, M. R., and Fares, E., "Simulation-Based Airframe Noise Prediction of a Full-Scale Full Aircraft," AIAA Paper 2016-2706, May-June 2016.

[3] Fares, E., Duda, B., and Khorrami, M. R., “Airframe Noise Prediction of a Detailed Full Aircraft in Model and Full Scale Using a Lattice Boltzmann Approach,” AIAA Paper 2016-2707, May-June 2016.
[4] Khorrami, M. R., Fares, E., Duda, B., and Hazir, A., “Computational Evaluation of Airframe Noise Reduction Concepts at Full Scale,” AIAA Paper 2016-2711, May-June 2016.
[5] Appelbaum, J., Duda, B., Fares, E., and Khorrami, M. R., "Airframe Noise Simulations of a Full-Scale Aircraft," AIAA Paper 2018-2973, June 2018.
[6] Ferris, R. J., Appelbaum, J., and Khorrami, M. R., "Simulations of a Full-Scale Aircraft with Installed Airframe Noise Reduction technologies," AIAA Paper 2018-2974, June 2018.
[7] Duda, B., Ferris, R. J., and Khorrami, M. R., “Simulation-Based Assessment of a Full-Scale Installed Quiet Landing Gear,” Paper to be presented at the AIAA/CEAS Aeroacoustics Conference in Delft, The Netherlands, May 2019.
[8] Khorrami, M. R., Lockard, D. P., Humphreys, W. M. Jr., and Ravetta, P. A., “Flight-Test Evaluation of Airframe Noise Mitigation Technologies,” AIAA paper 2018-2972, June 2018.
[9] Baumann, E. and Waggoner, E., “Flight and Ground Operations in Support of Airframe Noise Reduction Tests,” AIAA paper 2018-2970, June 2018.
[10] Khorrami, M. R., Lockard, D. P., Humphreys, W. M. Jr., and Ravetta, P. A., “Flight-Test Evaluation of Landing Gear Noise Reduction Technologies,” Paper to be presented at the AIAA/CEAS Aeroacoustics Conference in Delft, The Netherlands, May 2019.
[11] Humphreys, W. M. Jr., Lockard, D. P., Khorrami, M. R., Culliton, W. G., McSwain, R. G., Ravetta, P. A., and Johns, Z., “Development and Calibration of a Field-Deployable Microphone Phased Array for Propulsion and Airframe Noise Flyover Measurements,” AIAA Paper 2016-2898, May-June 2016.
[12] Ravetta, P., A., Wisda, D. M., Khorrami, M. R., and Van de Ven, T., “Assessment of Airframe Noise Reduction Technologies Based on EPNL from Flight Tests,” Paper to be presented at the AIAA/CEAS Aeroacoustics Conference in Delft, The Netherlands, May 2019.
[13] Khorrami, M. R., Ravetta, P. A., Lockard, D. P., Duda, B., and Ferris, R., "Comparison of Measured and Simulated Acoustic Signatures for a Full-Scale Aircraft with and without Airframe Noise Abatement," AIAA Paper 2018-2975, June 2018.
[14] Farassat, F. and Succi, G. P., “The Prediction of Helicopter Discrete Frequency Noise,” *Vertica*, Vol. 7, No. 4, pp. 309-320, 1983.
[15] Hawking, J. E., and Ffowcs Williams, D. L., “Sound Generation by Turbulence and Surfaces in Arbitrary Motion,” *Philosophical Transactions of the Royal Society of London, Series A, Mathematical and Physical Sciences*, Vol. 264, No. 1151, 1969, pp. 321–342.
[16] Najafi-Yazdi, A., Brès, G. A., and Mongeau, L., “An Acoustic Analogy Formulation for Moving Sources in Uniformly Moving Media,” *Proceeding of The Royal Society of London A*, Vol. 467 (2125), pp. 144-165, 2011.
[17] AVEC Time Domain Beamforming Software, Ver 2.70, AVEC, Inc., Blacksburg, VA, URL: http://www.avec-engineering.com/products.html [cited Oct 1, 2018].
[18] ICAO, Environmental Protection, Annex 16 to the Convention on International Civil Aviation, Vol. 1: Aircraft Noise, Appendix 2, July 2012.
[19] Federal Aviation Administration, “Noise Standards: Aircraft Type and Airworthiness Certification,” Advisory Circular No. 36-4D, October 12, 2017.